Computation of Incompressible Viscous Flow around a Marine Propeller

by Shotaro Uto*, *Member*

Summary

This paper describes an application of CFD (Computational Fluid Dynamics) to the computation of incompressible viscous flow around a marine propeller. High Reynolds-number flow around a marine propeller operating in a uniform flow is simulated using a newly developed CFD scheme, which is based on cell-centered, finite-volume method with global conservation property for mass and momentum flux.

Governing equations are full Navier-Stokes equations and continuity equation with pseudo-compressibility, which are written in boundary-fitted curvilinear coordinate system fixed on a propeller blade. For discretization in space, 3rd-order upwind scheme derived from flux-difference splitting method is adopted for convection terms and 2nd-order central difference scheme for viscous terms, respectively. 1st-order Euler implicit scheme is adopted for the time integration and the resulted discretized equations are solved by Implicit Approximate Factorization (IAF) scheme with high efficiency.

A series of high Reynolds-number flow computations around a SEIUNMARU conventional propeller are made to show validity and availability of the present scheme as a practical design tool. Through quantitative comparison of the computed results with experimental data for surface pressure distributions, thrust and torque coefficients, it is clearly shown that present scheme can predict a viscous flow around a marine propeller qualitatively well and that several problems, such as open boundary conditions and excessive grid skewness, should be solved in order to improve accuracy of the present scheme.

By flow visualization technique using the computed results, some important characteristics of a rotating propeller flow such as the development of boundary layers and separation on a propeller blade, tip vortex generation and a structure of trailing vortices, are found to be well simulated qualitatively by the present scheme, which may be useful tool for the development of the inviscid-flow calculation method.

1. Introduction

A lot of researchers and engineers have been engaged in the development of theories and computational methods of a propeller flow. Excellent works have been made to establish a practical calculation method of the steady and the unsteady propeller performance by lifting surface or lifting body theory[1)2)3)4)], etc. However, most of their works are based on the inviscid flow approximation, and some important aspects on the role of viscosity have been neglected or treated approximately. That means, problems such as a scale effect on model-ship correlation, nonlinear interaction between cavitation and viscous flow, and the structure and mechanism of boundary layer and vortical wake flow of a rotating propeller, have been left unsolved quantitatively. Especially, through further understanding on the structure of trailing vortices, it is expected to improve accuracy of the estimation of the propeller performance by an inviscid-based calculation method[3)]. The main and final objective of the present study is to simulate incompressible viscous flow around a marine propeller quantitatively both at model and full scale Reynolds number by CFD (Computational Fluid Dynamics) and to obtain comprehensive understanding on these unsolved problems.

Recent progress on the computer hardware and software has made it possible to compute a discretized Navier-Stokes equations directly to simulate three-dimensional viscous flow even using a desk-top workstation. In aeronautics, turbulent flow simulations around an ATP (Advanced Turbo Prop) had already been attempted successfully by CFD[5)]. However, challenges on the application of CFD to the flow computation around a marine propeller had been very limited so far. Stern et. al. successfully showed nonlinear interac-

* Ship Research Institute

Received 10th July 1992
Read at the Autumn meeting 9, 10th Nov. 1992

tion mechanism between a ship and a propeller, where a propeller was idealized to the body force distribution[6] or a rectangular plate with infinite pitch[7], Kato et. al.[8] computed cavitating flow around a finite-span hydrofoil to show the possibility of simulating a propeller flow including sheet, cloud and tip-vortex cavitation by CFD. Although these studies suggested the possibility and availabity of CFD, difficulties on the grid generation around a marine propeller prevented them from the practical CFD simulation. Uto et. al.[9] developed a new grid generation system using Implicit Geometrical method[10] and calculated a Euler inviscid flow around a propeller with relatively large pitch ratio, to suggest the possibility of the practical CFD simulation of a rotating propeller flow.

In this study, a series of CFD computations by cell-centered, finite-volume, upwind scheme are presented for the incompressible viscous flow around a marine propeller with a practical configuration. Formulation and computational scheme are based on the references[9][11]. Computed results are compared quantitatively with the experiment data[12] on surface pressure distributions, thrust and torque coefficients, to investigate validity and availability of the present scheme as a practical design tool. Furthermore, by flow visualization using the computed results, it is clearly shown that some important characteristics of a rotating propeller flow, such as the development of boundary layers on a propeller blade, separation, tip-vortex generation, and trailing vortex systems, are simulated qualitatively well.

2. Formulation

2.1 Coordinate systems and grid generation

In this section, three kinds of coordinate systems for describing a propeller flow are presented.

Fig. 1 shows a Cartesian coordinate system (O-xyz) fixed on a propeller blade, which is rotating clockwise with constant angular velocity (Ω). Origin (O) is fixed at the center of a propeller and the x-axis is measured along a propeller shaft which is positive in downstream direction. The z-axis points upward and the y-axis completes a right-handed coordinate system. Velocity components (u, v, w) are defined in (x, y, z) directions, respectively. It should be noticed a hub is idealized to the cylinder with a constant radius as shown in Fig. 1.

A cylindrical coordinate system (O-$xr\theta$) is also defined for convenience to present the computed results in section 3. The r-axis is a radial coordinate measured from x-axis and angluar coordinate θ is measured along the counter-rotating direction of a propeller.

The third one is a boundary-fitted curvilinear coordinate system (ξ, η, ζ) generated at the pre-processing, grid generation stage. The detail of the grid generation process should be referred to Uto et. al.[9] and Kodama[10]. It should be noticed that in this study H-H type is adopted as topology of the grid system. Fig. 2 shows a perspective view of the ξ-η plane including a suction side surface. The ξ-axis nearly coincides with a pitch line defined by a propeller geometry and positive in downstream direction. The η-axis nearly corresponds to

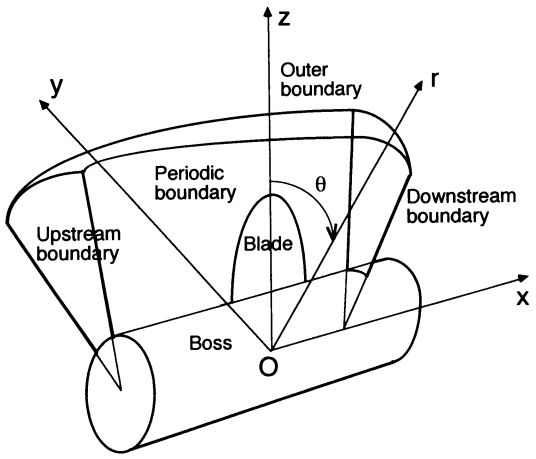

Fig. 1 Coordinate systems and boundaries around a propeller

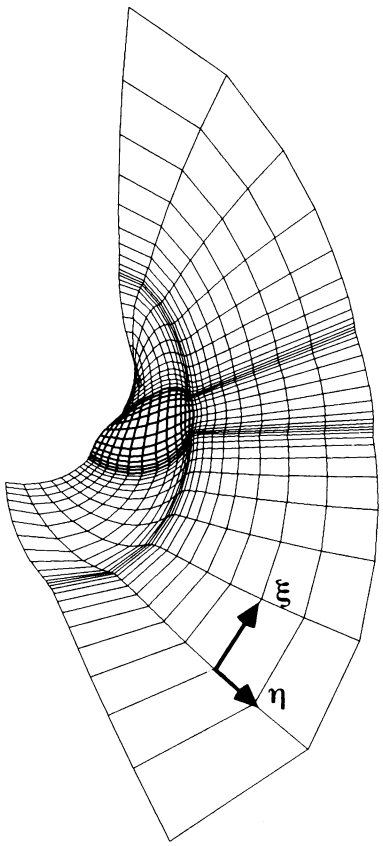

Fig. 2 Perspective view of grid around a propeller ($\xi-\eta$ plane, including a suction side surface)

the radial coordinate. Near the leading edge, trailing edge, tip and root of a blade, grid points are clustered as shown in Fig. 3, especially in order to simulate steep changes of the pressure field there. The ζ-axis makes a circumferential coordinate between two pitch-surfaces including a suction and a pressure surface of a propeller blade. Fig. 4 illustrates a η-ζ plane at the mid-chord position of a propeller blade. It is shown that grid points are also clustered in ζ-direction at the vicinity of a blade, in order to simulate the boundary layer flow developing on a blade surface with high resolution.

2.2 Governing equations and coordinate transformation

Governing equations are incompressible Navier-Stokes equations and continuity equation in conservation form, which are written by Cartesian coordinate system fixed on a rotating blade as follows.

$$\frac{\partial q}{\partial t}+\frac{\partial E}{\partial x}+\frac{\partial F}{\partial y}+\frac{\partial G}{\partial z}+\frac{\partial Ev}{\partial x}+\frac{\partial Fv}{\partial y}+\frac{\partial Gv}{\partial z}-H=0 \tag{2.1}$$

$$q=\begin{bmatrix}u\\v\\w\\p\end{bmatrix}\quad E=\begin{bmatrix}u^2+p\\uv\\uw\\\beta u\end{bmatrix}\quad F=\begin{bmatrix}uv\\v^2+p\\vw\\\beta v\end{bmatrix}\quad G=\begin{bmatrix}uw\\vw\\w^2+p\\\beta w\end{bmatrix}$$

$$Ev=-\frac{1}{Re}\begin{bmatrix}2u_x\\u_y+v_x\\u_z+w_x\\0\end{bmatrix}\quad Fv=-\frac{1}{Re}\begin{bmatrix}u_y+v_x\\2v_y\\v_z+w_y\\0\end{bmatrix} \tag{2.2}$$

$$Gv=-\frac{1}{Re}\begin{bmatrix}u_z+w_x\\v_z+w_y\\2w_z\\0\end{bmatrix}\quad H=\begin{bmatrix}0\\-2\Omega w+\Omega^2 y\\2\Omega v+\Omega^2 z\\0\end{bmatrix}$$

where all variables are non-dimensionalized using axial inflow velocity (U_{in}), a diameter of a propeller (D) and density of fluid (ρ), and Reynolds Number is defined as follows.

$$Re=\frac{U_{in}D}{\nu}=Rn\times J,\quad Rn=\frac{nD^2}{\nu},\quad J=\frac{U_{in}}{nD} \tag{2.3}$$

Pseudo-compressibility is introduced to the continuity equation in order to make a system hyperbolic and to compute velocity and pressure field at the same stage. However, contribution of it vanishes after the steady-state solution is attained. β is a pseudo-compressibility parameter and fixed to 1 in this study. The last term of the left-hand side of Eq. (2.1) is a source term derived from rotation of a propeller.

By coordinate transformation of the independent variables in Eq. (2.1) from Cartesian (O-x, y, z) to the boundary-fitted coordinate system (O-ξ, η, ζ), the following equations can be obtained.

$$V\frac{\partial q}{\partial t}+\frac{\partial \hat{E}}{\partial \xi}+\frac{\partial \hat{F}}{\partial \eta}+\frac{\partial \hat{G}}{\partial \zeta}+\frac{\partial \hat{E}v}{\partial \xi}+\frac{\partial \hat{F}v}{\partial n}+\frac{\partial \hat{G}v}{\partial \zeta}-VH=0 \tag{2.4}$$

where, V denotes a local volume of a control-volume and numerical fluxes are defined as follows.

$$\begin{bmatrix}\hat{E}\\\hat{F}\\\hat{G}\end{bmatrix}=\begin{bmatrix}(\delta Sn_x)^{\xi} & \delta Sn_y)^{\xi} & (\delta Sn_z)^{\xi}\\(\delta Sn_x)^{\eta} & (\delta Sn_y)^{\eta} & (\delta Sn_z)^{\eta}\\(\delta Sn_x)^{\zeta} & (\delta Sn_y)^{\zeta} & (\delta Sn_z)^{\zeta}\end{bmatrix}\begin{bmatrix}E\\F\\G\end{bmatrix},$$

similarly in $\hat{E}v$, etc. (2.5)

In Eq. (2.5), $(\delta Sn_x)^{\xi}$ denotes a x-projection of the cell interface area in ξ-direction and other metrices are defined similarly.

2.3 Discretization

Cell-centered, finite-volume, 3rd-order upwind scheme with global conservation property is adopted for the discretization of Eq. (2.4). Details of the discretization in space and time are described in reference[9] for 3-dimensional Euler inviscid flow and in reference[11] for 2-dimensional viscous flow. Therefore, only the outline is presented below.

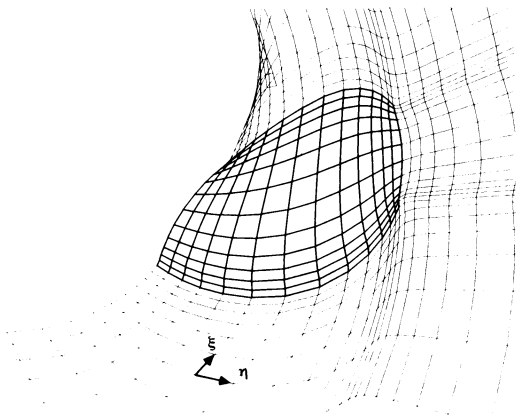

Fig. 3 Close view of grid around a propeller

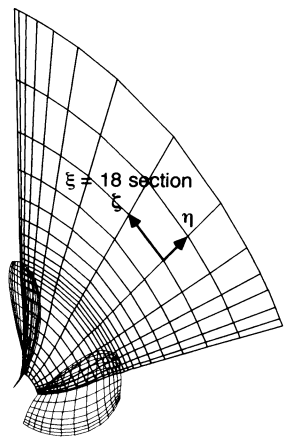

Fig. 4 Perspective view of grid around a propeller ($\eta-\zeta$ plane, mid-chord section)

Firstly, spatial differentiation of numerical fluxes in Eq. (2.4) can be replaced by 2nd-order central difference scheme to obtain a following equation.

$$V_{ijk}\frac{\partial q}{\partial t}+(\hat{E}+\hat{E}v)_{i+1/2}+(\hat{F}+\hat{F}v)_{j+1/2}+(\hat{G}+\hat{G}v)_{k+1/2}-(\hat{E}+\hat{E}v)_{i-1/2}-(\hat{F}+\hat{F}v)_{j-1/2}-(\hat{G}+\hat{G}v)_{k-1/2}-V_{ijk}H_{ijk}=0 \quad (2.6)$$

where (i, j, k) denotes as indices in (ξ, η, ζ) direction, respectively.

For the estimation of inviscid fluxes at the cell interface such as $\hat{E}_{i+1/2}$, 3rd-order upwind scheme based on flux-difference splitting method[11] is adopted. In case of viscous fluxes ($\hat{E}v_{i+1/2}$, etc.), 2nd-order central difference scheme is used. Time integration of the resulted semi-discrete form is made by first-order Euler implicit scheme. Discrete equations are factorized in ξ, η, ζ directions and solved efficiently by Implicit Approximate Factorization (IAF) method.

2.4 Boundary conditions

Fig. 1 shows a computational domain and boundaries around a propeller. Upstrem (S_u) and downstream boundary (S_d) is set about 1/2 pitch upstream and downstream of a propeller, respectively. Outer boundary (S_o) diameter is taken about three times as large as a propeller diameter. In the present study, computational domain has periodicity corresponding to the number of blades, because a propeller is assumed to operate in a uniform flow. So periodic boundaries (S_{p1}, S_{p2}) have to be newly introduced in a computational domain. It should also be noticed that in the computation a propeller blade (S_{bp}; pressure side, S_{bs}; suction side) is set at the center of periodic boundaries, which is not as shown in Fig. 4. As discussed in section 2.1, hub (S_h) is made of a cylindrical surface with a constant radius.

Boundary conditions are listed in Table 1. After several kinds of conditions at the upstream, downstream and outer boundaries had been tried, the following combination was found to be good for accuracy and stability of the computation. At the upstrem and the outer boundaries, velocity components are fixed as a uniform flow value, but pressure is extrapolated by zero -gradient from interior domain. On the other hand, at the downstream boundary pressure is fixed to zero and velocity components are zero-extrapolated from upstream points.

Table 1 Boundary conditions

Boundary	Boundary condition
Upstream (S_u)	u,v,w fixed $p_\xi=0$
Downstream (S_d)	$u_\xi=v_\xi=w_\xi=0$ p fixed
Outer (S_o)	u,v,w fixed $p_\xi=0$
Hub (S_h)	$u_\eta=v_\eta=w_\eta=p_\eta=0$ (free slip)
Periodic (S_{p1},S_{p2})	continuity and conservation of mass and momentum
Blade (S_{bp},S_{bs})	u=v=w=0 $p_\zeta=0$ (Non slip)

At the periodic boundaries, continuity and conservation of mass and momentum fluxes are satisfied[13] to take account of the future extension of the present scheme using a "multi-block" type grid[14]. However, this type of the boundary condition may cause degradation of the numerical stability to some extent, because the explicit treatment is inevitably needed at the periodic boundary.

Non-slip condition is given on a propeller blade, but Kutta condition is not used at the tip and the trailing edge, which is indispensably used by the inviscid flow calculation. On the other hand, a hub surface is treated as a free-slip wall in order to avoid exessive grid clustering near a hub surface and to save a CPU time. Therefore in this computation, no hub-vortex system is simulated.

3. Computed Results and Discussions

3.1 General conditions

A model propeller used for the present study is a Conventional Propeller (CP) designed for a training ship "SEIUN MARU". Principal particulars of this propeller are presented in Table 2. Open-water characteristics and pressure distributions on a propeller blade were measured at Ship Research Institute[12] and several organizations and reliability of the experimental data is thought to be high enough.

Table 3 shows basic computational conditions. Reynolds number (Re) is relatively low compared to the model scale($Re=O(10^5)$) or full scale ($Re=O(10^7)$), so the laminar flow over a propeller blade is simulated in this study. Two kinds of grid systems, coarse and fine grid are used, where a propeller blade is subdivided by 11 (chordwise) $\times$ 9 (spanwise) and 13×15 panels, respectively. Minimum grid spacing in ζ-direction is 0.001, which corresponds to $0.1/\mathrm{Re}^{1/2}$, to compute the boundary layer flow developing on a propeller blade with high resolution. Computations are made in the range of relatively large advance coefficient (J), because the laminar flow separation occurs easily at the backside of a propeller blade and the steady-state solution cannot be obtained at smaller J-value. Maximum time step ($\Delta t_{\max}$) is 0.003 (coarse grid) and 0.0015 (fine), and after about 3000 iterations, the $L2$-norm of Δq is decreased to less than $O(10^{-6})$ and the difference of the computed forces is within 1% between by momentum integral at outer boundaries and by surface stress integral[11]. A CPU time per iteration is about 21 seconds (coarse grid) and 33 seconds (fine) by IBM Powerstation 320.

3.2 Perspective view of the computed flow over a propeller blade

In this subsection, the computed propeller flow over a

Table 2 Principal particulars of a model propeller

Propeller	Seiun maru CP
Pitch ratio	0.950
E.Area ratio	0.650
Boss ratio	0.1972
No. of blades	5
Skew angle	10.5°
Rake angle	6.0°
Blade section	MAU

Table 3 Basic computational conditions

Reynolds No.	10000
Grid size	$\xi \times \eta \times \zeta$
Coarse grid	33×20×15 11×9 on Blade
Fine grid	37×26×15 13×15 on Blade
Min.Spacing	0.001
Advance coef.	$0.7 \leqq J \leqq 1.0$
Max. Δt	0.0015~0.003

blade is presented in detail by flow visualization, to show and to discuss some important characteristics of the viscous flow around a marine propeller.

Figs. 5 and 6 show a perspective view of the computed pressure distribution on the two pitch surfaces, which include a suction and a pressure side of a propeller blade, at $J=0.7$ and $J=0.9$, using a fine grid. Pressure coefficient (C_p) is defined by the following relation.

$$C_p=\frac{p-p_{in}}{1/2\rho n^2 D^2} \tag{3.1}$$

where p_{in} denotes an averaged pressure at the upstream boundary. In these figures, full and dotted lines indicate positive and negative pressure region respectively and a contour interval (ΔC_p) is 0.2.

It is clearly shown in these figures that negative pressure contours are stretched toward a trailing edge at the vicinity of the blade tip on a suction side, which suggests flow separation and tip-vortex generation. On the pressure side, pressure oscillation is observed locally at the trailing edge of the blade tip. It is thought that a kink of the grid line and insufficient grid density may cause such pressure oscillation there. At $J=0.9$, pressure distributions are more moderate than those at $J=0.7$, especially near the leading edge and the blade tip.

Figs. 7 and 8 show a plot of "limiting" velocity vectors just over a propeller blade at $J=0.7$ and $J=0.9$, respectively. Limiting velocities are defined as those at the nearest grid point over a blade surface in ζ-direction. It is clearly shown that the low momentum fluid within the boundary layer is forced to convect outside radially under the influence of the centrifugal force, and that such behavior is more remarkable at $J=0.7$ than at $J=0.9$. Near the tip at the trailing edge, flow vectors are found to be disordered, mainly because of the pressure

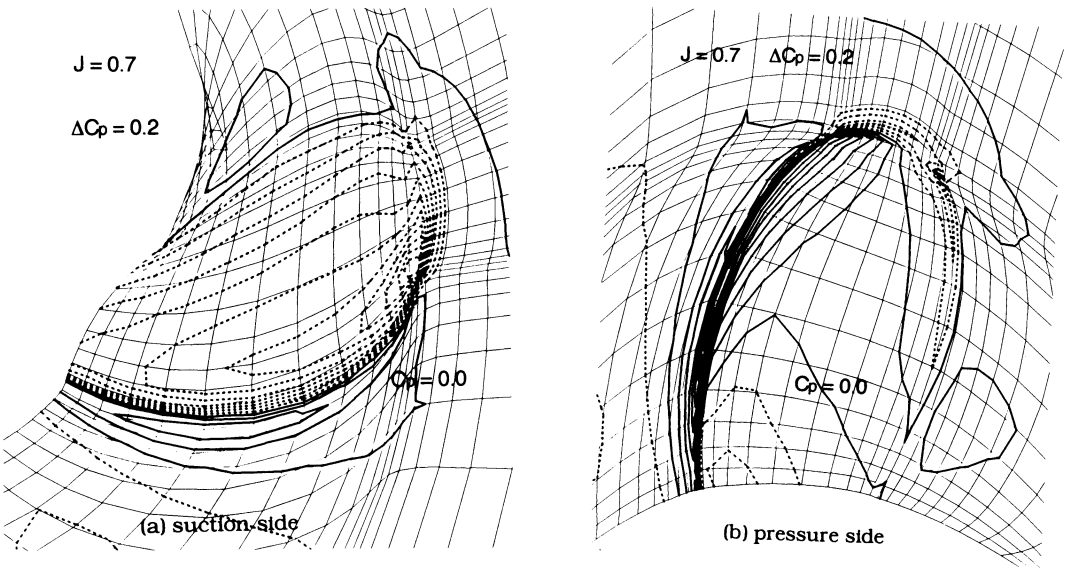

Fig. 5 Pressure distribution around a propeller ($J=0.7$)

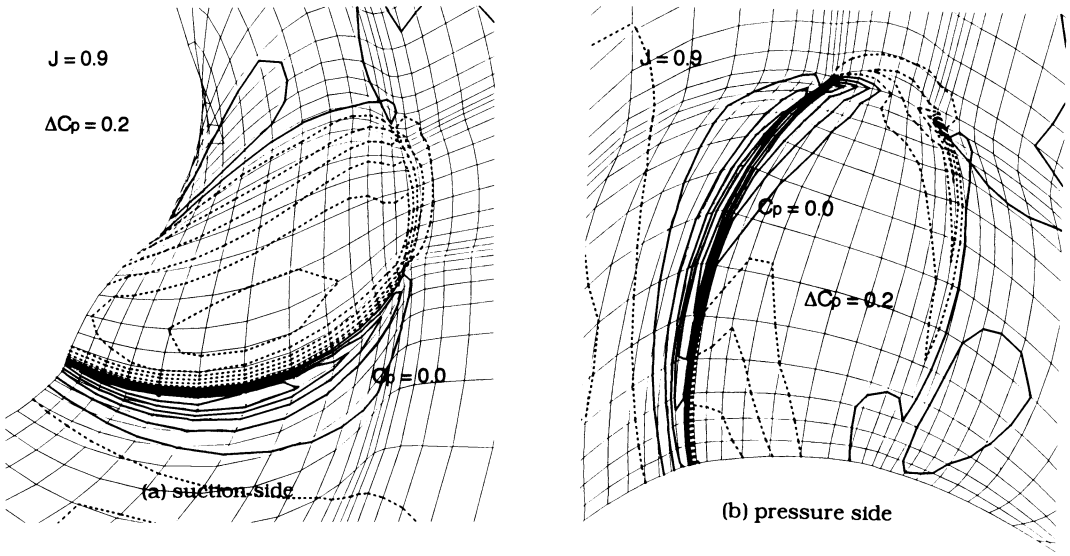

Fig. 6 Pressure distribution around a propeller ($J=0.9$)

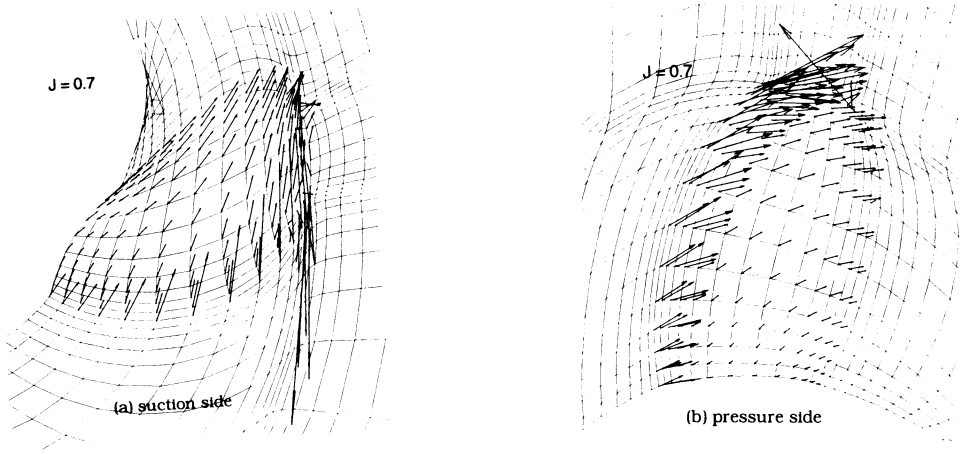

Fig. 7 Limiting velocity distribution on a propeller blade ($J=0.7$)

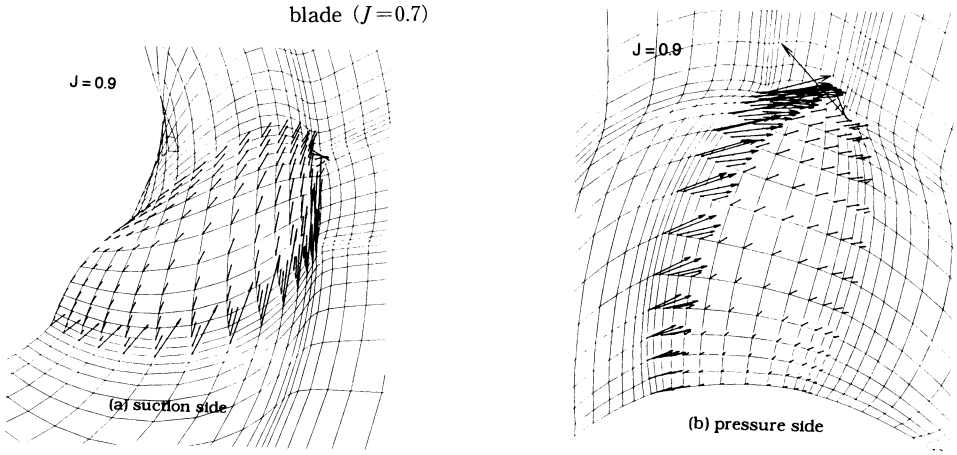

Fig. 8 Limiting velocity distribution on a propeller blade ($J=0.9$)

oscillation discussed above. Moreover at $J=0.7$, local flow separation is observed near the leading edge of the suction side.

The development of boundary layers are well observed by contour plots of the speed magnitude $((u^2+v^2+w^2)^{1/2})$ at the circumferential, blade to blade section (ξ=constant plane). From Figs. 9 to 11, contour plots at $\xi=12$ (just after leading edge), $\xi=18$ (mid-chord) and $\xi=23$ (just before trailing edge) sections are presented at $J=0.7$, where a contour interval is 0.5. It can be observed the clear distinction of the development of boundary layers between a suction and a pressure side, especially near the blade tip. That means the boundary layer is more developed on a suction side surface and that contour lines are gradually shifted circumferentially upward near the tip of a suction side to indicate generation and roll-up process of the tip vortex system. However, more detailed discussions on the boundary layer flow should be restrained because of the insufficient grid density in ζ-direction.

3.3 Structure of the trailing vortices

One of the main target of the propeller flow simulation by CFD is to get comprehensive information and understanding on the trailing vortices, in order to enhance the accuracy of the performance estimation by inviscid flow calculation method[3]. Therefore pressure contours at four ξ=constant sections (see Fig. 12) are presented from Figs. 13 to 16 ($J=0.7$, fine grid). In these figures, full and dotted lines indicate positive and nega-

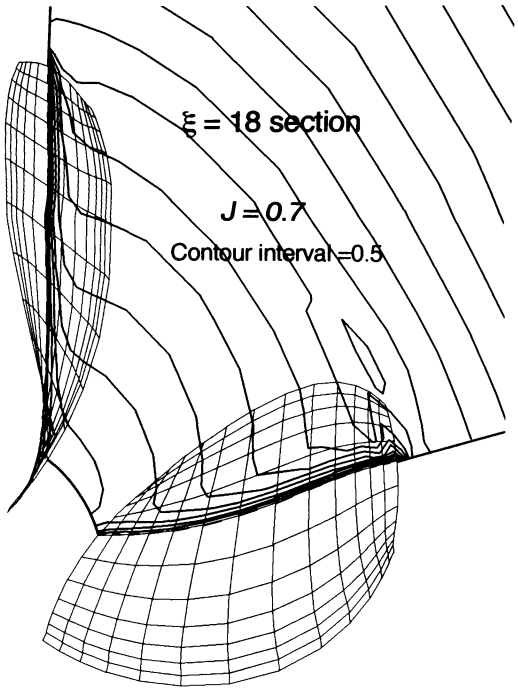

Fig. 10 Speed magnitude contours at the mid-chord section ($\xi=18$)

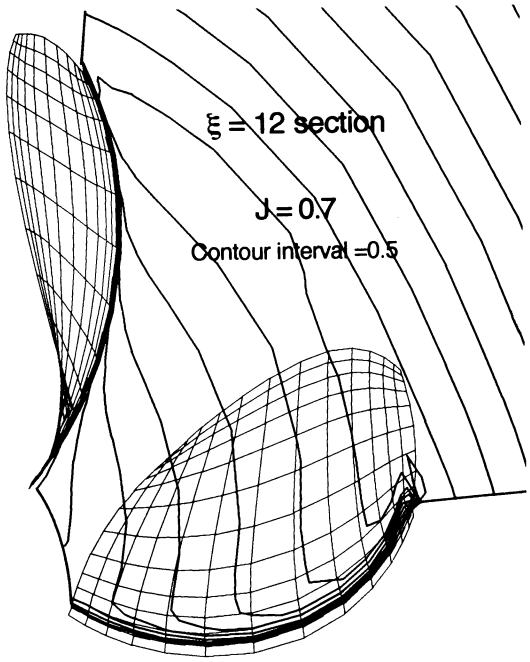

Fig. 9 Speed magnitude contours at the leading edge section ($\xi=12$)

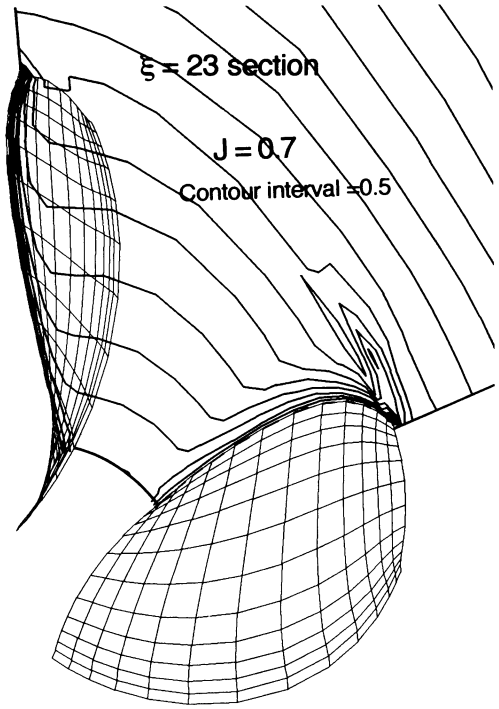

Fig. 11 Speed magnitude contours at the trailing edge section ($\xi=23$)

tive pressure region respectively and a contour interval (ΔC_p) is 0.2.

It can be clearly seen that a low-pressure core region, which corresponds to the tip-vortex system, is stretched circumferentially and convected to downstream. The hydrodynamic pitch angle of the core center are found to be relatively small compared to a geometical pitch angle. In order to validate this tendency and to understand a detail structue of trailing vortices, pitch angles of circumferentially averaged trailing vortices , β_w, is plotted against a radial position in Figs. 17 ($J=0.7$) and 18 ($J=0.9$) at three wake sections. β_w and β_G (a geometrical pitch angle) are defined as follows.

$$\beta_w=\tan^{-1}\left(\frac{\bar{u}}{\bar{u}_\theta}\right) \tag{3.2}$$

$$\beta_G=\tan^{-1}\left(\frac{P(r)}{2\pi r}\right) \tag{3.3}$$

where $\bar{u}$ and $\bar{u}_\theta$ mean a circumferentially averaged axial and tangential velocity, respectively and $P(r)$ denotes a radial pitch distribution of a propeller.

It is shown in these figures that near the tip β_w becomes smaller than β_G, which corresponds to the above mentioned, and that β_w at $J=0.7$ is much smaller than that at $J=0.9$ near the tip. The same tendency was observed in the experiment[3] by LDV and that assures the validity of the present scheme.

3.4 Surface pressure distribution

The surface pressure distribution is one of the most essential parameters for design and analysis of a marine propeller. In this section, quantitative comparison of the computed surface pressure with experiment data[12] is presented in order to make validation of the present

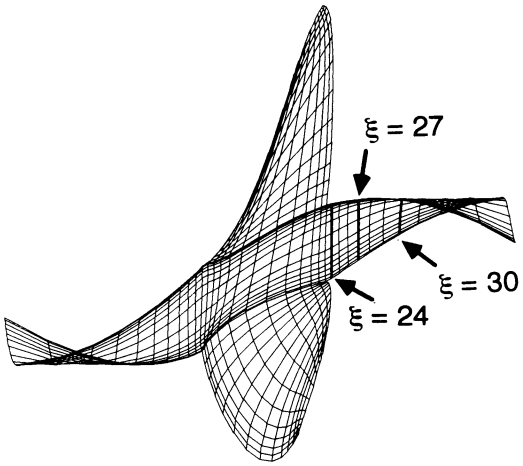

Fig. 12 Location of the wake sections (ξ=const. section)

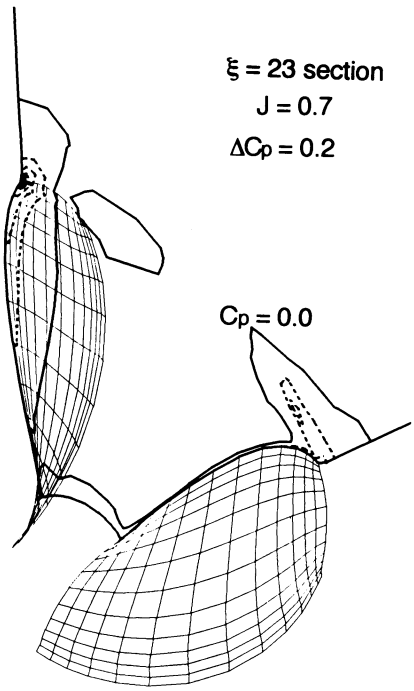

Fig. 13 Pressure distribution at the trailing edge section (ξ=23)

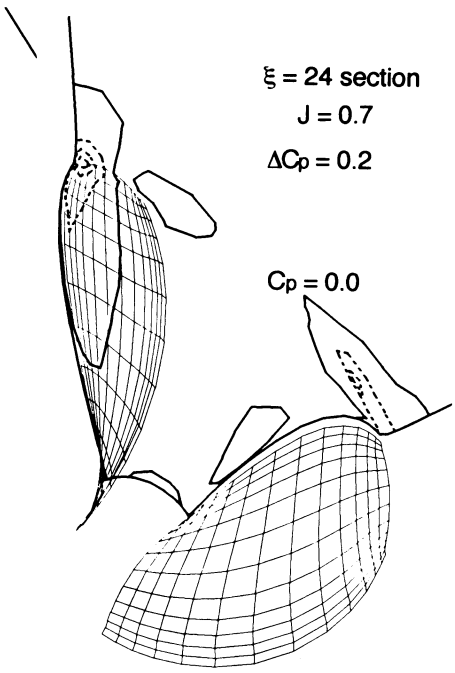

Fig. 14 Pressure distribution at the wake section (ξ=24)

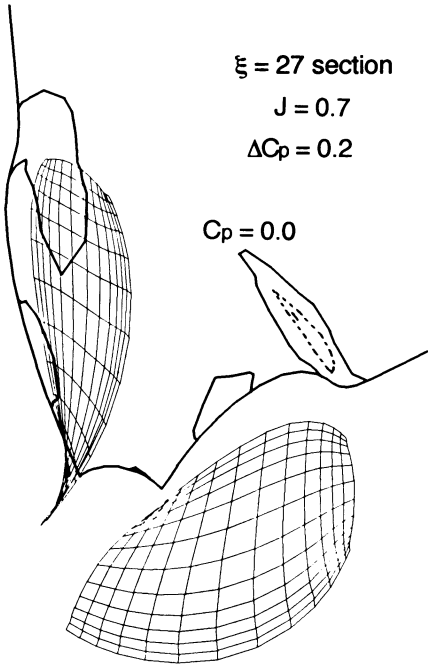

Fig. 15 Pressure distribution at the wake section ($\xi=27$)

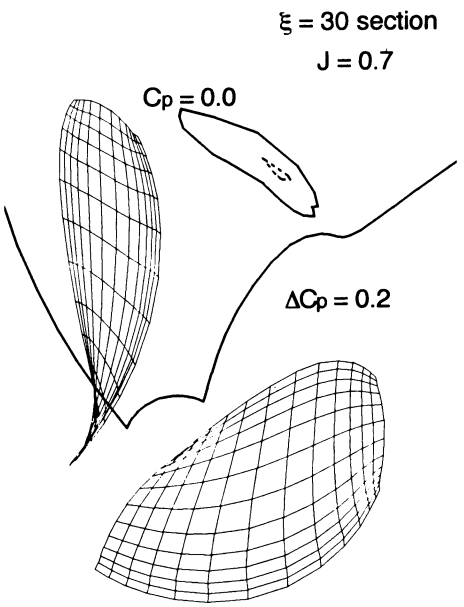

Fig. 16 Pressure distribution at the wake section ($\xi=30$)

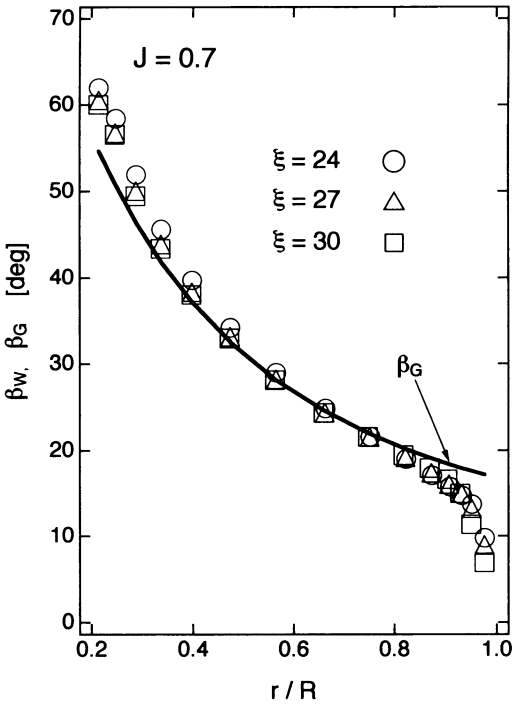

Fig. 17 Radial distributions of a pitch angle of trailing vortices ($J=0.7$)

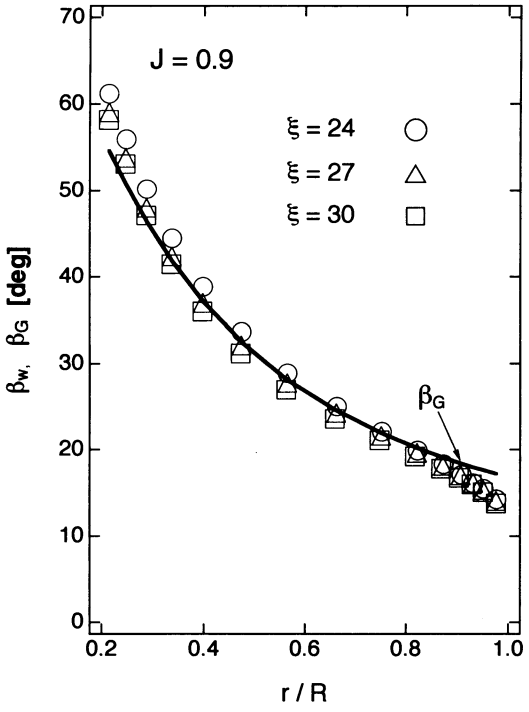

Fig. 18 Radial distributions of a pitch angle of trailing vortices ($J=0.9$)

scheme.

Figs. 19 and 20 show radial (at $x=0.4$ c) and chordwise (at $r=0.7$ R) pressure distributions at $J=0.7$, using a fine grid, respectively. In case of the radial pressure distribution, better agreement is observed quantitatively at the suction side than at the pressure side, and the same tendency was reported for the computed results using lifting surface theory[12]. The distinctive behavior on both sides at the tip should also be remarked. On the other hand, in case of the chordwise pressure distribution, the discrepancy near the leading edge is found to be relatively large. The main factors of this discrepancy may be due to the insufficient grid density and the grid skewness near the leading edge, and the latter is inevitably brought by a conventional "single-block" grid around a marine propeller with a practical configuration. Other factors are presented and discussed in section 3.5.

3.5 Thrust and Torque coefficients

Open water characteristics are of great importance from an engineering standpoint. Therefore in this section, by comparing the estimated thrust (K_T) and torque coefficients (K_Q) with experiment data, further validation of the present scheme is proceeded. It should be noticed that K_Q is calculated only from the pressure contribution because the Re discrepancy affects K_Q value greatly.

Fig. 21 shows a comparison of the computed K_T and K_Q with experiment data. Good agreement is shown qualitatively, but the computed results are estimated about 20% higher than experiment data even in case of fine-grid simulations. And the difference between the two increases as J gets higher except at $J=0.7$, where local separation occurs at the suction side (fine grid) or steady-state solution cannot be obtained (coarse grid). To explain this discrepancy, the following factors are presented and discussed below.

Effect of the grid size

Fig. 21 also shows the effect of the grid size on the computed results of K_T and K_Q. Clearly, the results using a finer grid system show better agreement with the experiment data. However, even in case of the fine grid, the grid density is not enough, especially in ζ-direction. Therefore simulations with finer grid system should be needed to make further validation of the grid size effect on the present scheme.

Effect of Reynolds number

The next and important factor is the Reynolds Number (Re) effect. Generally, this effect is thought to be negligible if $Rn(=nD^2/\nu)$ is higher than about 5×10^5. And in the range below this Rn, both K_T and K_Q tend to increase gradually as Rn higher. However, such monotonic dependence may not be guaranteed through the transition point from laminar (present results) to turbulent flow. Therefore, turbulent flow simulations are indispensable in order to validate the Re-effect on this problem.

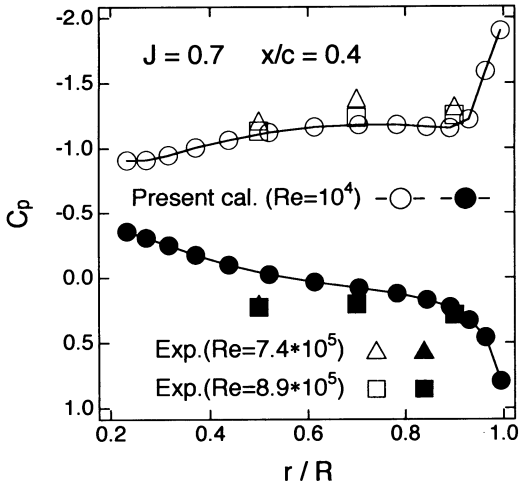

Fig. 19 Comparison of radial pressure distribution ($J=0.7$, $x=0.4$ c)

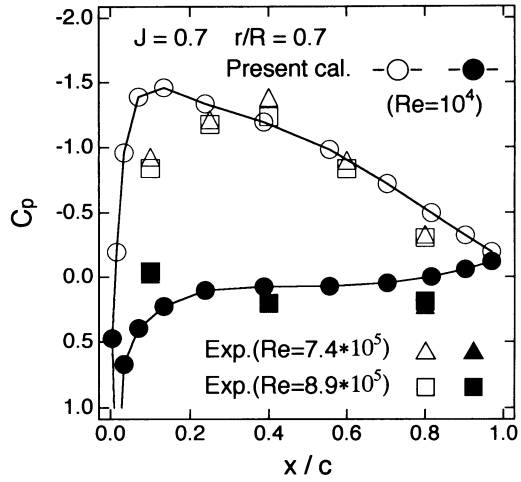

Fig. 20 Comparison of chordwise pressure distribution ($J=0,7$, $r=0.7$ R)

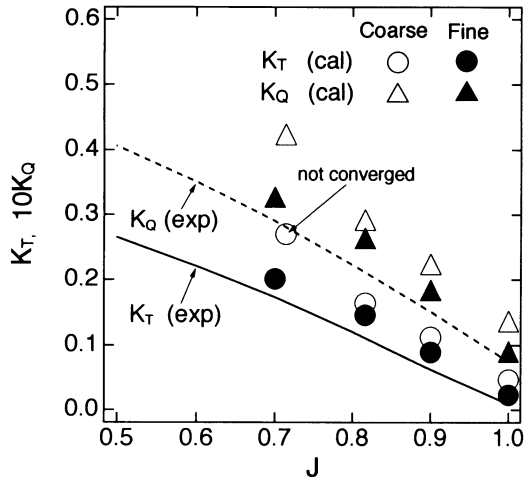

Fig. 21 Comparison of thrust and torque coefficients

For reference, Table 4 shows a Re-effect of the computed results in the laminar flow region, using a fine grid. They show the same Re-dependency as the above mentioned, which is composed of the increase of K_{TP}, the contribution of surface pressure integral under the influence of the displacement effect of the boundary layer, and the decrease of $-K_{TV}$, the contribution of viscous stress. That may suggest the reliability of the present scheme.

Table 4 Effect of Reynolds number on open water characteristics

Re	KT	KTP	KTV	KQ	ηo
1×10^4	0.0892	0.1089	-0.0197	0.01838	0.6952
2×10^4	0.1087	0.1226	-0.0139	0.01984	0.7848
3×10^4	0.1143	0.1257	-0.0114	0.02028	0.8073

(J=0.9, by fine grid)

Effect of outer boundary

In the experiment at a cavitation tunnel, a side-wall effect is one of the important factors to influence on the measured K_T and K_Q[12]. In this computation, outer boundary is treated like a "free-slip" rotating wall, as mentioned in section 2.4. Therefore, the side wall effect due to the finite radius of outer boundary (So) may cause over-estimation of open water characteristics. In order to investigate this effect, a simulation using the grid system with outer boundary radius 30% larger is tried but little changes on the computed K_T and K_Q values are observed. So it is concluded this effect is negligible in this computation.

Effect of upstream boundary

The finite region of the computational domain may also influence on the upstream, uniform flow condition. In the present scheme, inflow velocity field is fixed at the upstream boundary, which is set about only 1/2 diameter upstream of a propeller. Taking into account the effect of the induced velocity field at the upstream boundary (U_{induced}) is included in this fixed velocity components, the true inflow velocity field at the infinite, far-field boundary (U_∞) should be given as follows.

$$U_\infty = U_{\text{in}} - U_{\text{induced}} \tag{3.4}$$

Therefore, J value must be decreased according to the above U-correction. This factor can explain well the reason for discrepancy between the computed and experiment data qualitatively. In order to avoid this error, inflow boundary must be set as far upstream as possible from a propeller, but that is not a good solution from an economical aspect. Instead, matching with the computed results by the inviscid flow calculation method at the upstream boundary is recommended.

4. Concluding Remarks

(1) Using a newly-developed CFD scheme based on cell-centered, finite-volume method, high Reynolds -number laminar flow around a marine propeller with a practical configuration is simulated around a SEIUN-MARU conventional propeller at relatively high advance coefficient.

(2) By quantitative comparison between the computed results and experiment data, validity of the present scheme is discussed in detail. It is shown that the present scheme can predict open water characteristics (K_T and K_Q) qualitatively well but about 20% higher than experiment data, and that the surface pressure are over-predicted at both sides near the leading edge.

(3) The main reasons of these discrepancies are found to be,

(a) grid skewness near the leading edge and kinks near the blade tip,

(b) insufficient grid size,

(c) open boundary condition, especially upstream boundary condition

(4) As a remedy of them, the followings are recommended.

(a) use of "multi-block" grid,

(b) further improvement of stability and efficiency of the present scheme,

(c) matching with the computed results by the inviscid flow computational scheme as open boundary conditions.

(5) In order to simulate a propeller flow at smaller J and at model and full scale Reynolds number, turbulence model suitable for the rotating propeller flow should be developed and introduced in the present scheme.

(6) By flow visualization using the computed results, it is found that some important characteristics of a rotating propeller flow, such as the development of boundary layers on a propeller blade, separation, tip-vortex generation, and trailing vortex systems, are simulated qualitatively well.

Acknowledgments

The author would like to express his sincere gratitude to the member of CFD group, Dr. Kodama, Dr. Hinatsu, Mr. Murata, Mr. Harumi, Mr. Hirata, and Dr. Liu at Ship Research Institute for their valuable discussions and suggestions. The author also would like to acknowledge the continuing encouragement by Dr. Kitagawa and Dr. Koyama, and the presentation of valuable experiment data by Dr. Ukon at SRI. The present work could not have been accomplished without cooperation by his colleagues, Mr. Yoshida, Mr. Izumiyama, Mr. Kanada, Mr. Shimoda and Mr. Tabuchi at SRI Ice Tank.

References

1) Hoshino, T.: "Propeller Theory" (in Japanese), Proceedings of the third Symposium on Marine Propellers (1987), pp. 23-95.

2) Hoshino, T.: "Hydrodynamic Analysis of Propeller in Steady Flow Using a Surface Panel

Method", Journal of SNAJ, Vol. 165 (1989), pp. 55-70.
3) Hoshino, T.: "Hydrodynamic Analysis of Propellers in Steady Flow Using a Surface Panel Method, 2nd report: Flow Field around Propeller", Journal of SNAJ, Vol. 166 (1989), pp. 79-92.
4) Koyama, K.: "Application of a Panel Method to the Unsteady Hydrodynamic Analysis of Marine Propellers", Proceedings of 18th ONR symposium (1992).
5) Matsuo, Y. et. al.: "Navier-Stokes Simulations of Flows around a High-Speed Propeller", Proceedings of 3rd Int. Sym. Comput. Fluid Dynamics, (1989), pp. 523-529.
6) Stern, F. et. al.: "A Viscous Flow Approach to the Computation of Propeller-Hull Interaction", Journal of Ship Research, Vol. 32 (1988), pp. 246-262.
7) Stern, F. et. al.: "Computation of Viscous Flow around a Propeller-Shaft Configuration with Infinite-Pitch Rectangular Blades", Proceedings of 5th Int. Conf. Numerical Ship Hydrodynamics, (1989), pp. 408-423.
8) Kato, H. et. al.: "Finite Difference Calculation of Cavitating Flow around a Finite Span Hydrofoil" (in Japanese), Journal of SNAJ, Vol. 168 (1990), pp. 97-104.
9) Uto, S. et. al.: "Application of CFD to the Flow Computation Around a Marine Propeller -Grid Generation and Inviscid Flow Computation using Euler Equation-" (in Japanese), Journal of KSNAJ, Vol. 218 (1992), to be published.
10) Kodama Y.: "Grid Generation around a Practical Ship Hull Form Using the Implicit Geometrical Method", (in Japanese), Journal of SNAJ, Vol. 169 (1991), pp. 27-38.
11) Kodama, Y.: "A Cell-Centered, Finite-Volume Upwind Scheme with Global Conservation", Journal of SNAJ, Vol. 168 (1990), pp. 21-30.
12) Ukon, Y. et. al.: "Measurement of Pressure Distribution on a Conventional and a Highly Skewed Propeller Model -Under Non-Cavitating Condition-", (in Japanese), Journal of SNAJ, Vol. 165 (1989), pp. 83-94.
13) Uto, S. et. al.: "Computation of the Two-Dimensional Viscous Flow around a Wing Section in Cascade with Composite Grid Method" (in Japanese), Journal of KSNAJ, Vol. 215 (1991), pp. 61-67.
14) Uto, S. et. al.: "Composite Grid Simulation of Incompressible Flow around a Propeller" (in Japanese), Proceedings of the 58th General Meeting of SRI, (1991), pp. 43-46.